AN INVESTIGATION OF LIQUID METAL AND GAS FLOW CHARACTERISTICS IN CONFINED ATOMIZATION NOZZLE

Assit.Prof.Dr.Ihasn Y.Hussain
Mech.Engr.Dept.
College of Engineering
University of Baghdad
Baghdad-Iraq.

ABSTRACT

Supersonic gas jets in confined liquid metal atomizing nozzle were studied by using the method of characteristics. Nitrogen at operation (stagnation) pressure of (1.65Mpa) was used in the study, with three different values of ambient pressure (1.25, 1.52 and 1.75 bar). For all the three values, the nozzle is over expanded. The Mach number at the nozzle exit for all the investigated cases was (2.64). The pressure and Mach number of the atomizing gas at various lattice points downstream of the nozzle exit were found. Besides, the effect of heat transfer from the liquid metal (aluminum) on the gas flow behavior was also investigated. The results showed that the stagnation temperature rise of nitrogen caused by heat transferred from aluminum is very small and can be neglected, and hence the flow can be assumed to be adiabatic. The results indicates that the pressure of the atomizing gas tries to adjust to the higher ambient pressure by the formation of a weak oblique "lip" shock followed by a reflected weak oblique "edge" shock. As the ambient pressure increases, the inward curvature of the jet boundary increases and hence the length of the jet decreases. As the ambient pressure increases, the point at which the oblique "lip" shock strikes the wall moves upstream toward the nozzle exit. If the shock is to be avoided, the difference between the ambient and nozzle exit pressures must be decreased. For fixed nozzle geometry, this can be done either by increasing the operation pressure or by decreasing the ambient pressure.

الخلاصة

في هذا البحث، تمت دراسة نفاث الغاز فوق الصوتي الخارج من منفث التذرية للسوائل المعدنية باستخدام طريقة المميزات. الغاز المستعمل كان النيتروجين عند ضغط تشغيلي (ساكن) مقداره (1.56Mpa)، مع ثلاث قيم للضغط الجوي خارج المنفث (1.25,1.52,1.75 bar). لكل هذه القيم الثلاثة كان المنفث مفرط الاتساع ورقم ماخ عند مقطع الخروج للمنفث كان (2.64). تم احتساب الضغط ورقم ماخ عند مختلف نقاط الشبكة بعد المنفث، بالإضافة إلى ذلك، تمت دراسة تأثير انتقال الحرارة من السائل المعدني (الالومينا) إلى الغاز (النتروجين). بينت النتائج ان الارتفاع في درجة حرارة الركود للغاز (النتروجين) بسبب الحرارة المنتقاة إليه من السائل المعدني (الالومينا) كان صغيراً ويمكن إهماله وافتراض ان جريان الغاز أديباتي. أظهرت النتائج ان ضغط الغاز المتذري يحاول ان يصل إلى قيمة الضغط الجوي العالي خارج المنفث عن طريق تكوين صدمة "شفة" مائلة عند مخرج المنفث تتبعها صدمة "حافة" مائلة منعكسة من جدار الأنبوب. زيادة الضغط الجوي خارج المنفث تسبب زيادة تقوس حدود النفاث الخارجية باتجاه الداخل، ونتيجة لذلك يقل

طول النفاث، كما ان زيادة الضغط الجوي يدفع نقطة اتصال صدمة "الشفة" المائلة بجدار الأنبوب إلى الخلف باتجاه المنفث. إذا ما اريد تجنب حصول الصدمة، فان الفرق بين الضغط الجوي وضغط مخرج المنفث يجب ان يقل، وهذا يمكن تحقيقه أما بزيادة ضغط التشغيل (الركود) أو بتقليل الضغط الجوي، أو كلاهما.

KEY WORDS
Atomization Nozzle Liquid Metal, Gas Flow Method of Characteristics

INTRODUCTION

Confined atomization nozzle is usually used for producing fine powders of reactive metals, such as aluminum and magnesium. The atomization gas issues as a high velocity jet and act as a jet pump causing the breakup of the liquid metal and powder formation (Unal,1987). In this designs the annular channel is placed around a central tube which protrudes a certain distance beyond it, as shown in **Fig.(1)**. The atomizing gas issues from the annulus as a high velocity jet and contacts the liquid metal around the tip of the central tube (delivery tube) through which it is introduced. It is known that the formation of powder particles takes place by disintegration during flight in the gas jet of relatively large liquid droplets obtained at the first point of contact around the delivery tube (Ynal, 1987 and Unal, 1989 and Klar&Fesko,1984).

The influence of the nozzle geometry in this process had been studied by (Unal, 1988).

The present paper investigates the liquid metal (aluminum) and gas (Nitrogen) flow characteristics in a confined converging-diverging nozzle. The nozzle considered in this work is shown in **Fig.(1)**. It consists of straight metal delivery tube surrounded by annular gas channel. The delivery portion of the gas channel is of conical taper. The details of the nozzle setup and its dimensions are shown in **Fig.(1)**. The throat area is ($16.49mm^2$) and the exit area is ($50mm^2$). The Nitrogen mass flow rate is (1Kg/min). This nozzle is similar to the one investigated experimentally by (Unal, 1989).

Heat Transfer Model

The effect of heat transfer from the liquid metal (aluminum) to the gas (nitrogen) through the delivery tube was investigated by using a simplified mode. The target was the calculation of the gas stagnation temperature rise caused by this heat transfer.

As the flow path is short, the heat transfer rate (q) from the liquid metal (aluminum) to the delivery tube and to the gas (nitrogen) is governed by the following relation (Holamn,1981) see **(Fig.2)**;

$$q = \frac{T_{Al} - T_{nit.}}{\frac{1}{h_{Al} 2\pi r_1 L} + \frac{\ln(r_2 / r_1)}{2\pi k L} + \frac{1}{h_{nit.} 2\pi r_2 L}} \qquad (1)$$

where(T_{Al},T_{int},h_{Al} and h_{int}) are the liquid metal and gas temperature and heat transfer coefficients respectively; (k) is the thermal conductivity of the delivery tube wall.

In the proposed design, the stagnation inlet temperature of the nitrogen is (300-325K). Based on this value, the nitrogen temperature was taken as (T_{int}=300K), to be in the safe side in the calculations. The inlet temperature of the liquid metal in the proposed design is (760°C), and it must remains liquid along the delivery tube, i.e., the minimum temperature should not be less than (660°C), the melting point of aluminum. We use (T_{Al}=760°C=1033K) in the calculations.

To calculate the heat transfer coefficient of nitrogen (h_{nit}), Sieder and Tate correlation for turbulent flow (Holamn, 1981) was used;

$$St.Pr^{2/3} = 0.023\ Re^{-0.2} \qquad (2)$$

and for the liquid metal heat transfer coefficient (h_{Al}), the following empirical relation for constant heat flux and turbulent flow conditions (Holman,1981) was used;

$$Nu = 4.82 + 0.0185(Re\,Pr)^{0.827} \qquad (3)$$

Evaluating the nitrogen and aluminum properties at the appropriate reference temperatures, and using (530 m/s) and (0.5 m/s) as the average velocities of nitrogen and aluminum respectively, the heat transfer coefficients were calculated, and then, by using eq.(1) the heat transfer rate (q) was calculated to be (244.8W). based on this value, and on the following relation:

$$q = \dot{m} C_p \Delta To \quad (4)$$

the stagnation temperature rise (ΔTo) of the nitrogen was calculated to be approximately ($4^{\circ}C$), which is a very small value, and can be neglected, and the gas flow may be assumed to adiabatic.

NOZZLE FLOW

The investigated nozzle is very short, and its walls are smooth. Hence the frictional effects may be neglected compared with the area change effects, and the gas flow may be assumed to be reversible. Therefore, and since the flow is adiabatic as it was proved in the previous section, the nitrogen gas flow may be treated as isentropic flow.

With exit to throat area ratio of (3), the exit Mach number can be found from the isentropic flow tables to be equal to (2.64), and the pressure ratio is (P/P_o=0.04711), where (P_o) is the stagnation (operation) pressure, which is equal to (1.56 Mpa) in the proposed design. Hence, the nozzle exit pressure will be (P_e=0.735 bar).

The ambient pressure ($P_{amb.}$) at the region downstream of the nozzle exit may have any value independent of the operation pressure and the exit Mach number. In the present work, three values for this pressure were investigated. These are (1.25,1.52 and 1.75 bar). In all the three cases, the nozzle is over expanded, since the exit pressure is smaller than the ambient pressure.

SUPERSONIC JET

The behavior of the supersonic jet of the nitrogen gas flow leaving the nozzle exit was investigated by using the method of characteristics (Shapiro,1953). This method may be employed to calculate the wave pattern and jet boundaries in the protrusion area. The following simplifying assumptions were made:

1- The annular nozzle is represented by a rectangular slit of height equal to the nozzle exit gap, i.e., two –dimensional flow.
2- The gas flow direction is parallel to the wall of the delivery tube on the inner side and to the outer nozzle wall on the outside, changing uniformly across the height of the slit.
3- Gas behaves as an ideal inviscid gas ($\gamma = 1.4$) for nitrogen.
4- The interaction between waves is neglected.

The starting point for the characteristics solution was the gas exit plane where the flow assumed to reach a uniform Mach number of (2.64). the method was then used for calculating flow conditions downstream of this line, as described in the following sections.

For two-dimensional irrotational flow, the compatibility equation are (Shapiro,1953);

$$\theta + \nu = \text{const.} = C_I \text{ (along right running Mach wave I)} \quad (5)$$

$$\theta - \nu = \text{const.} = C_{II} \text{ (along right running Mach wave II)} \quad (6)$$

In the present work, the Mach number was assumed to be (2.64) at points (1) through (6)(see **Figs.(3,4 and 5)**, and the flow direction to vary uniformly from (0deg.) at point (6) to (14.5) at point (1). This information is adequate to draw the characteristic starting from each of these six points, since the angles the characteristics make with the horizontal can now be calculated. For point (2), for example, these are;

Angle (2-7) with horizontal

$$\text{Type-II characteristics} = \theta_2 + \mu_2 \quad (7)$$

Angle (2-8) with horizontal

$$\text{Type-I characteristics} = \theta_2 - \mu_2 \quad (8)$$

Characteristics at points (1) through (6) may, therefore, be drawn. The interactions points of a type -I and type -II
Characteristics give points (7) through (11). This way solution progresses one step. At any point, and using **eqs.(5) and (6)**;

$$\theta = \frac{C_I + C_{II}}{2} \tag{9}$$

$$\nu = \frac{C_I - C_{II}}{2} \tag{10}$$

At point (12), the free stream boundary condition is applied that is, the pressure equal to the ambient pressure. Also, the C_{II} value is that of point (7). At point (17), the flow is parallel to the wall. Hence ($\theta = 0$), and the C_I value is that of point (11).
The coordinates (x_3,y_3) of any point (3) in the mesh can be calculated from the coordinates (x_1,y_1) and (x_2,y_2) of the two points (1 and 2) used to generate it by using the following relations;

$$x_3 = \frac{\left[y_2 - x_2 \tan\left(\overline{\theta+\mu}\right)_3\right] - \left[y_1 - x_1 \tan\left(\overline{\theta-\mu}\right)_3\right]}{\left[\tan\left(\overline{\theta-\mu}\right)_3\right] - \left[\tan\left(\overline{\theta+\mu}\right)_3\right]} \tag{11}$$

$$y_3 = \frac{\tan\left(\overline{\theta-\mu}\right)_3 \left[y_2 - x_2 \tan\left(\overline{\theta+\mu}\right)_3\right] - \tan\left(\overline{\theta+\mu}\right)_3 \left[y_1 - x_1 \tan\left(\overline{\theta-\mu}\right)_3\right]}{\left[\tan\left(\overline{\theta-\mu}\right)_3\right] - \left[\tan\left(\overline{\theta+\mu}\right)_3\right]} \tag{12}$$

Where:

$$(\theta-\mu)_3 = \frac{(\theta-\mu)_1 + (\theta-\mu)_3}{2} \tag{13}$$

$$(\theta+\mu)_3 = \frac{(\theta+\mu)_1 + (\theta+\mu)_3}{2} \tag{14}$$

Points (1) and (3) are along the same I-wave and points (2) and (3) are along the same II-wave.
The solution progresses this way. Mach numbers obtained in this solution may be converted to pressure using the isentropic flow tables.
When characteristics coalesce, an oblique shock wave is formed. If the oblique shock is relatively weak, it may be ignored without a serious error in the flow field calculations, since weak oblique shock waves yield an almost isentropic compression.
However, if the resulting oblique shock wave is very strong, it must be treated as a discrete finite discontinuity. In the present work, the internal shock waves indicated in (**Figs.3, 4 and 5**) were treated as weak shocks, and the characteristics were allowed to cross.

REULTS AND DISCUSSION

The pressure and Mach number of the atomizing gas at various lattice points downstream of the nozzle exit was found. The arrangement of the mesh on which the calculation were made, and the values of the Mach numbers and pressures at various lattice points are shown in (**Figs. 3,4 and 5**) for (1.25,1.52 and 1.75 bar) ambient pressures respectively. The details of the calculations results are also, given in (**Tables 1, 2 and 3**).
As the gas exit, the jet behaves like an under expanded flow and expands outward. This is clearly the result of the varying flow directions in the gas. The outer jet boundary bends inward to comply with the constant pressure in the ambient fluid, and the Mach number remains constant at the outer surface. Along the length of the protrusion, pressure decreases and Mach number increases, leading to increase flow velocities at a given section from the outer jet boundary towards the wall.
It is clear from the three figures, that in all the three cases, the pressure of atomizing gas tries to adjust to the higher ambient pressure by the formation of a weak oblique "lip" shock followed by a reflected weak oblique "edge" shock strikes the wall of the delivery tube at approximately the same

point ($x \approx 4.91$mm) or approximately at the tip of the delivery tube. As the ambient pressure increases, the strength of the oblique "lip" shock increases, and the Mach number at the lattice points behind the waves decreases and the pressure increases. As the ambient pressure increases, the inward curvature of the jet boundary increases and hence the length of the supersonic jet decreases. The point at which the oblique "lip" shock strikes the wall moves upstream toward the nozzle exit as the ambient pressure, the oblique "lip" shock will become a strong normal shock wave standling at the nozzle exit. The value of the ambient pressure required for this case was calculated to be (5.854 bar), which is a large value compared to the investigated values in the proposed design. Therefore, a change of the ambient pressure by small values above or below the design value will not cause noticeable changes.

If the shock is to be avoided, the difference between the ambient pressure ($P_{amb.}$) and the nozzle exit pressure (P_e) must be diminished, i.e., we must approach the fully expended zone of operation. For fixed nozzle geometry, i.e., fixed exit Mach number, this can be done either by increasing the operation (stagnation) pressure (P_o) or by decreasing the ambient pressure ($P_{amb.}$), or both, until the nozzle exit pressure and the ambient pressure become equal.

Concerning the effect of supersonic jet of the liquid metal atomizing process, it had been shown that along supersonic region in the jet is a prerequisite for the production of fine powder (**Unal, 1988**). Hence, and since the decreases in ambient pressure causes an increase in the supersonic jet, it is preferred to work with low ambient pressures.

CONCLUDING REMARKS

The method of characteristics has been applied for assessing the gas flow conditions in a given liquid metal atomizing nozzle. An oblique shock forms at the edge of the delivery tube (edge shock), and the wave pattern in the gas then operates in such a way as to turn the flow outward. This, in part, balances the inward pressure force of the annular jet. The length of the supersonic jet was found to increase as the ambient pressure decreases. Increasing the ambient pressure causes an increase in the inward curvature of the jet boundary, and the point at which the "lip" shock strikes the inner wall of the delivery tube to move upstream toward the nozzle exit.

REFERENCES

Holman ,J.P. (1981), Heat Transfer , McGraw Hill,.

Klar, E. and Feskow,W. (1984), Meatl Hanbook,.

Shapiro, A.H. (1953), The Dynamic and Thermodynamics of Compressible Fluid Flow,Vol.I,Ronald,Newyork,.

Unal,A.Mater.Sci.,Technol.,Vol.4,pp.1029-1039,1987.

Unal, A.Mater.Sci.,Technol.,Vol.4,pp.909-915,1988.

Unal, A.Metall.trans.B.,Vol.20B,pp.61-69,1989.

Unal, A., (1989), Influence of gas Flow on Performance of confined Atomization Nozzle, Metall.Trans.B, Vol.20B,833-843,.

NOMENCLATURE

(SI units are used, unless otherwise stated)

Symbol	Description
CI	Constant for type I- characteristics

CII	Constant for type II- characteristics
D	Diameter of the delivery tube
h	Protrusion length of delivery tube
h_{Al}	Heat transfer coefficient between liquid metal (aluminum) and delivery tube
K	Thermal conductivity of delivery tube wall
L	Length of delivery tube
M	Mach number
P	Pressure
$P_{amb.}$	Ambient pressure
P_e	Nozzle exit pressure
P_o	Operation (stagnation) pressure
Pr	Prandtl number
q	Heat transfer rate
r_1	Inner radius of delivery tube
r_2	Outer radius of delivery tube
Re	Reynolds number
St	Stanton number
T_{Al}	Liquid metal(aluminum) temperature
T_{nit}	Gas (nitrogen) temperature
T_o	Stagnation temperature
x	Exit gap
(x,y)	Coordinates of point
α	Angle of nozzle divergent region
μ	Mach angle ($\mathrm{Sin}^{-1}\frac{1}{M}$)
θ	Flow direction
ν	Prandtl Meyer angle

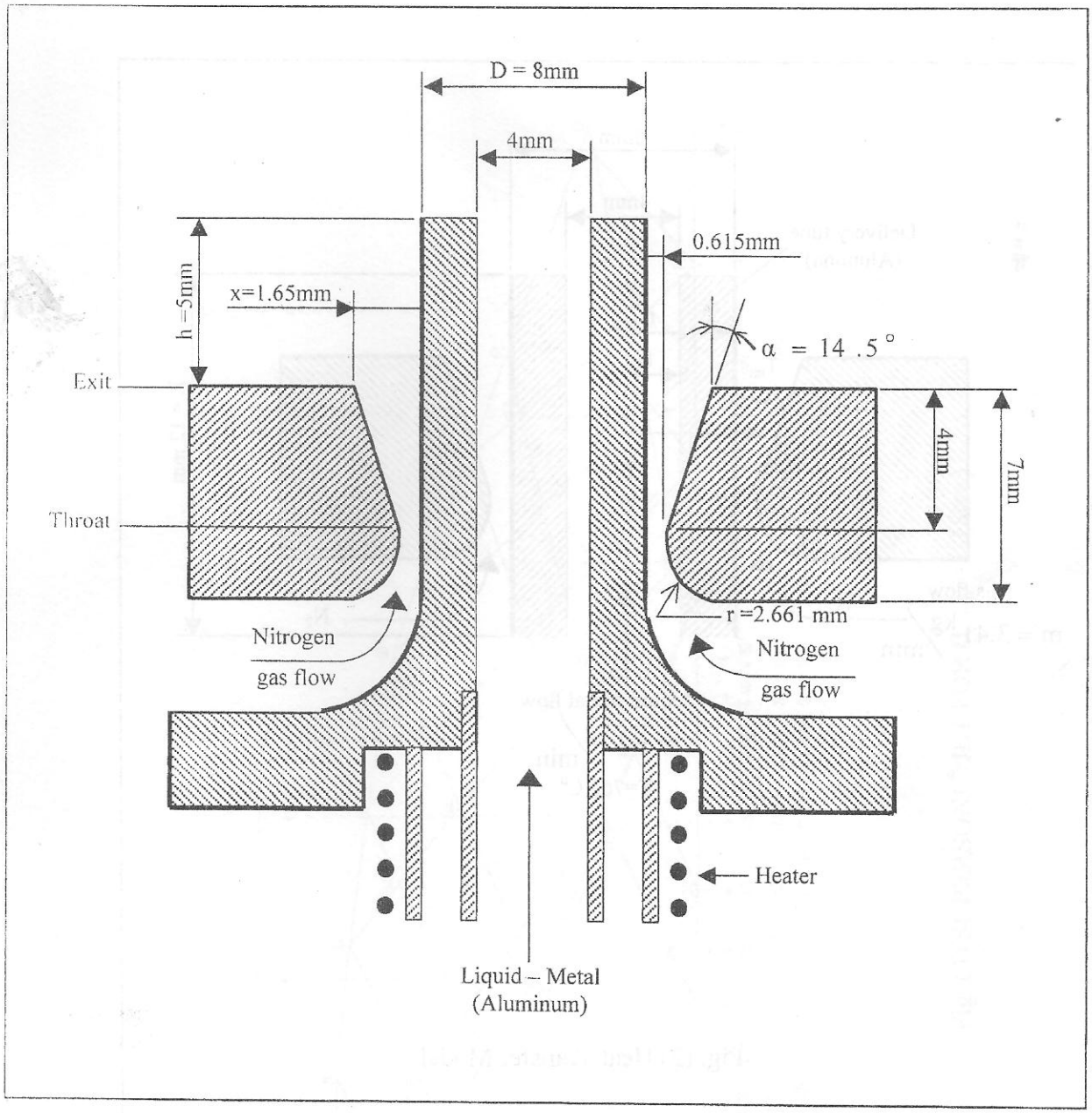

Fig. (1) Nozzle Geometry and Setup

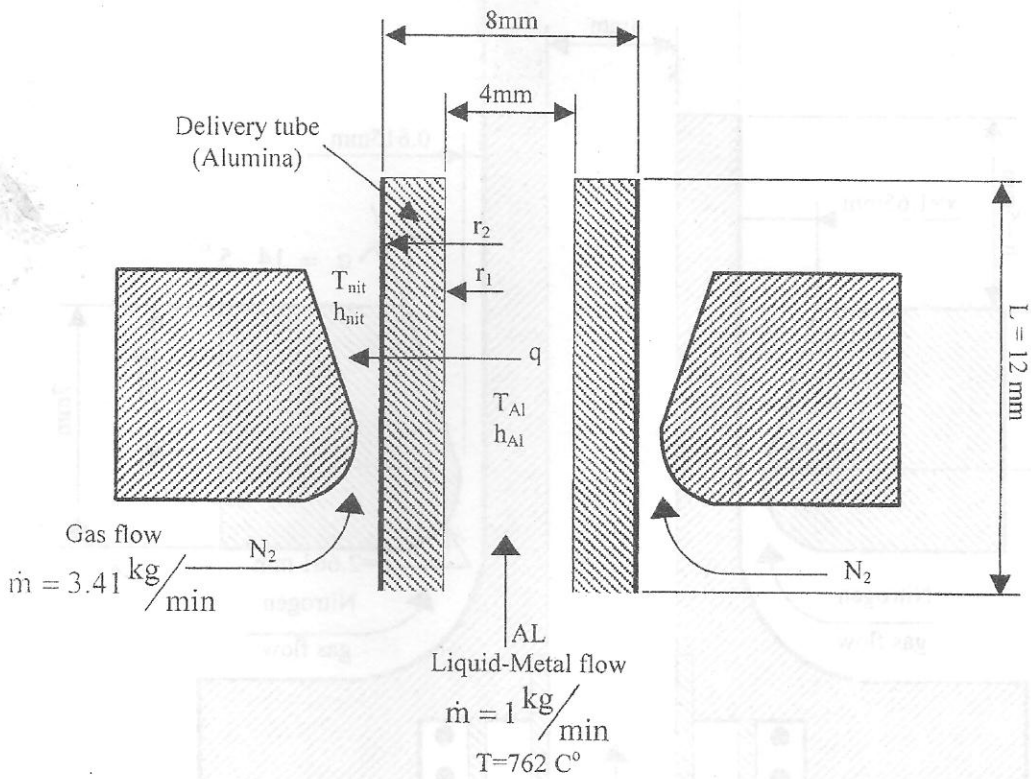

Fig. (2) Heat Transfer Model

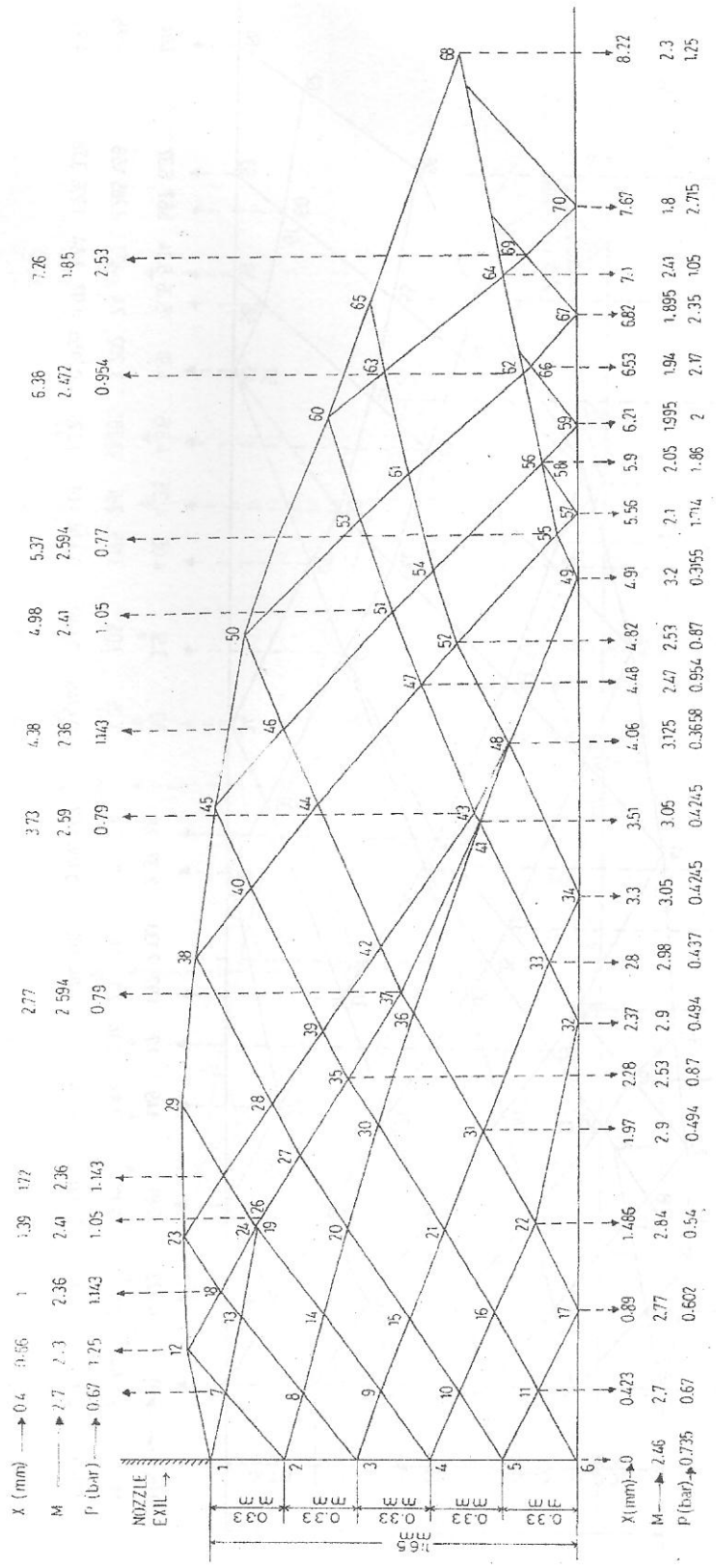

Fig. (3) SUPERSONIC JET FOR ($P_{amb.}$ =1.25bar)

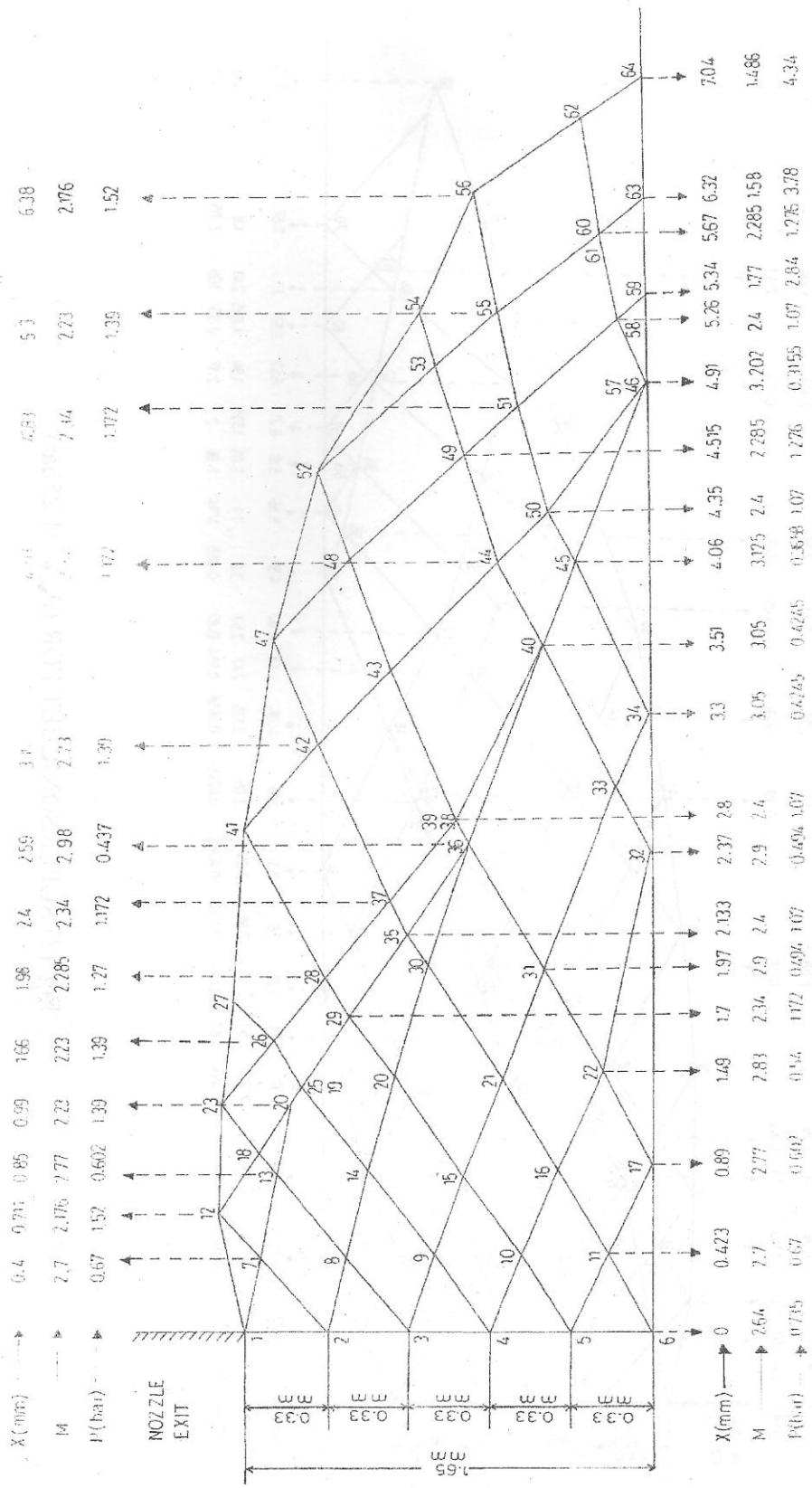

Fig. (4) SUPERSONIC JET FOR ($P_{amb.}$ =1.52bar)

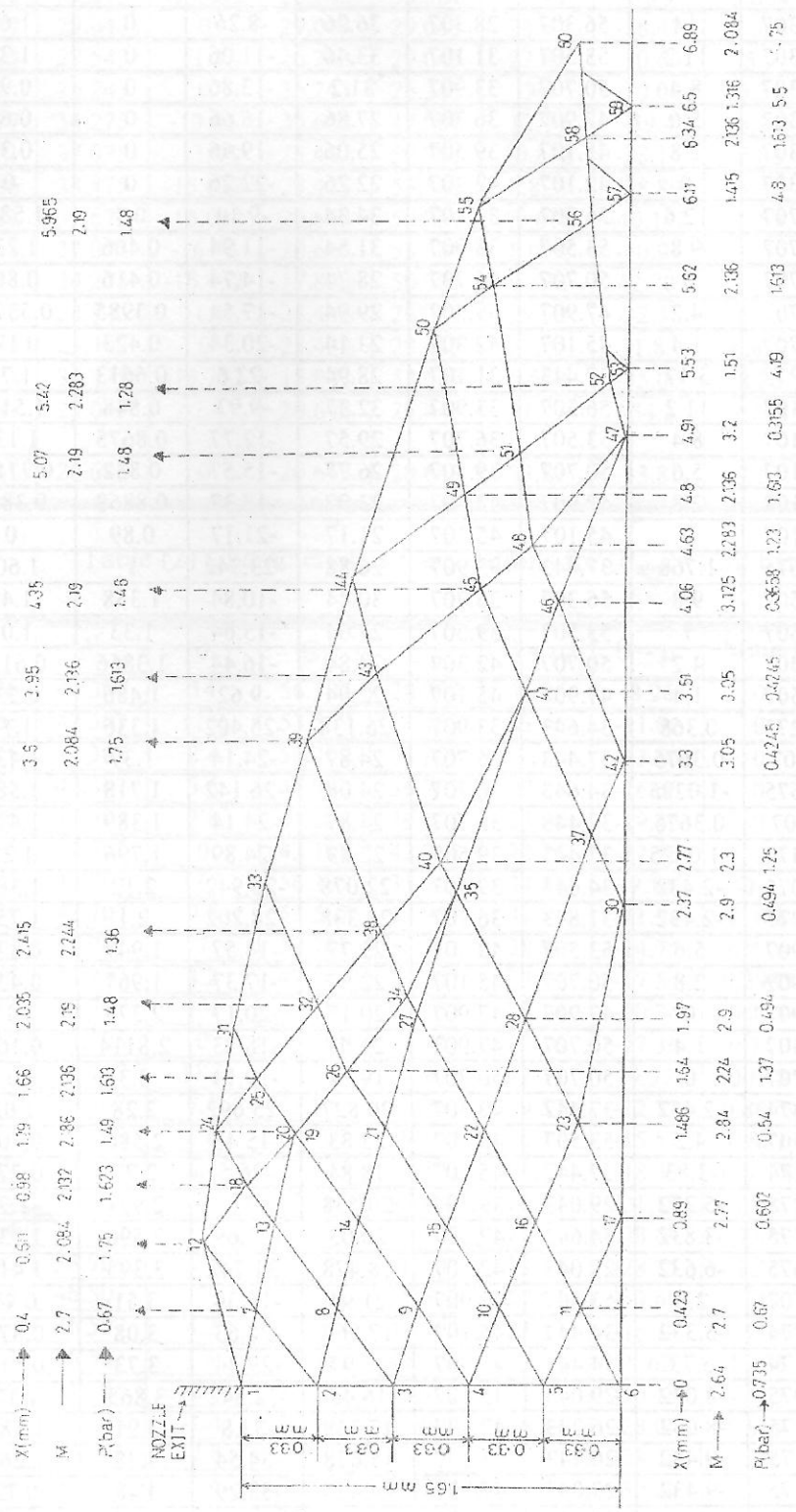

Fig. (5) SUPERSONIC JET FOR ($P_{amb.}$ =1.75bar)

Table (1) Characteristics Calculations for ($P_{amb.}$=1.25 bar)

Point No.	M	μ	ν	θ	C_I	C_{II}	θ+μ	θ−μ	X(mm)	Y(mm)	P(Mpa)
1	2.64	22.26	42.307	14	56.307	28.307	36.26	-8.26	0	1.65	0.0735
2	2.64	22.26	42.307	11.2	53.507	31.107	33.46	-11.06	0	1.32	0.0735
3	2.64	22.26	42.307	8.4	50.707	33.907	31.2	-13.86	0	0.99	0.0735
4	2.64	22.26	42.307	5.6	47.907	36.707	27.86	-16.66	0	0.66	
5	2.64	22.26	42.307	2.8	45.107	39.507	25.06	-19.46	0	0.33	0.0735
6	2.64	22.26	42.307	0	42.107	42.307	22.26	-22.26	0	0	0.0735
7	2.7	21.74	43.707	12.6	56.307	31.107	34.34	-9.14	0.4	1.5888	0.067
8	2.7	21.74	43.707	9.8	53.507	33.907	31.54	-11.94	0.406	1.237	0.067
9	2.7	21.74	43.707	7	50.707	36.707	28.74	-14.74	0.416	0.884	0.067
10	2.7	21.74	43.707	4.2	47.907	39.507	29.94	-17.54	0.3985	0.53743	0.067
11	2.7	21.74	43.707	1.4	45.107	42.307	23.14	-20.34	0.423	0.177	0.067
12	2.3	25.77	34.275	3.17	37.443	31.107	28.94	-22.6	0.6613	1.75	0.125
13	2.769	21.17	45.107	11.2	56.307	33.907	32.37	-9.97	0.848	1.5126	0.06018
14	2.769	21.17	45.107	8.4	53.507	36.707	29.57	-12.77	0.8675	1.136	0.06018
15	2.769	21.17	45.107	5.6	50.707	39.507	26.77	-15.57	0.832	0.77135	0.06018
16	2.769	21.17	45.107	2.8	47.907	42.307	23.97	-18.37	0.8868	0.3855	0.06018
17	2.769	21.17	45.107	0	45.107	45.107	21.17	-21.17	0.89	0	0.06018
18	2.356	25.11	35.675	1.768	37.443	33.907	26.88	-23.342	1	1.608	0.11428
19	2.836	20.64	46.507	9.8	56.307	36.707	30.44	-10.84	1.358	1.42	0.054084
20	2.836	20.64	46.507	7	53.507	39.507	27.64	-13.64	1.33	1.03	0.054084
21	2.836	20.64	46.507	4.2	50.707	42.307	24.84	-16.44	1.3866	0.6123	0.054084
22	2.836	20.64	46.507	1.4	47.907	45.107	22.04	-9.62	1.486	0.236	0.054084
23	2.3	25.77	34.275	0.368	34.643	33.907	26.138	-25.402	1.336	1.77	0.125
24	2.41	24.51	37.07	0.3675	37.443	36.707	24.87	-24.14	1.39	1.436	0.10505
25	2.356	25.11	35.675	-1.0325	34.643	36.707	24.08	-26.142	1.718	1.585	0.11428
26	2.41	24.51	37.07	0.3675	37.443	36.707	24.87	-24.14	1.389	1.435	0.10505
27	2.472	23.86	38.474	-1.0325	37.443	39.507	22.83	-24.89	1.796	1.25	0.095373
28	2.41	24.51	37.075	-2.432	34.643	39.507	22.078	-26.942	2.12	1.384	0.10505
29	2.3	25.77	34.275	-2.432	31.843	36.707	23.338	-28.202	2.1	1.756	0.125
30	2.9	20.17	47.907	5.6	53.507	42.307	25.77	-14.57	1.947	0.875	0.04937
31	2.9	20.17	47.907	2.8	50.707	45.107	22.97	-17.37	1.967	0.436	0.04937
32	2.9	20.17	47.907	0	47.907	47.907	20.17	-20.17	2.373	0	0.04937
33	2.977	19.63	49.307	1.4	50.707	47.907	21.03	-18.23	2.8114	0.165	0.043764
34	3.05	19.14	50.707	0	50.707	50.707	19.14	-19.14	3.3	0	0.04245
35	2.5325	23.26	39.874	-2.432	37.442	42.307	20.827	-25.692	2.28	1.02	0.086807
36	2.977	19.63	49.307	4.2	53.507	45.107	23.83	-15.43	2.586	0.704	0.043764
37	2.594	22.67	41.274	-3.83	37.442	45.107	18.84	-26.5	2.77	0.775	0.07891
38	2.3	25.77	34.275	-5.232	29.043	39.507	20.538	-31	2.931	1.7	0.125
39	2.472	23.86	38.475	-3.832	34.643	42.307	20.03	-27.69	2.596	1.138	0.095373
40	2.356	25.11	35.675	-6.632	29.043	42.307	18.478	-31.742	3.395	1.417	0.11428
41	3.05	19.14	50.707	2.8	53.507	47.907	21.94	-16.34	3.51	0.44	0.04245
42	2.528	23.3	39.774	-5.332	34.442	45.107	17.967	-28.63	3.08	0.878	0.087416
43	2.59	22.71	41.174	6.73	34.442	47.907	15.97	-29.44	3.73	0.516	0.079399
44	2.41	24.51	37.075	-8.032	29.043	45.107	16.48	-32.542	3.865	1.12	0.10505
45	2.3	25.77	34.275	-8.032	26.243	42.307	17.738	-33.8	3.91	1.586	0.125
46	2.356	25.11	35.675	-9.432	26.243	45.107	15.678	-34.54	4.38	1.268	0.11428
47	2.472	23.86	38.475	-9.432	29.043	47.907	14.428	-33.29	4.48	0.72	0.09573
48	3.125	18.66	52.107	1.4	53.507	50.707	20.06	-17.26	4.06	0.272	0.03658
49	3.202	18.21	53.507	0	53.507	53.507	18.21	-18.21	4.91	0	0.03155
50	2.3	25.77	34.275	-10.832	23.443	45.107	14.94	-36.602	4.925	1.417	0.125
51	2.41	24.51	37.075	-10.832	26.243	47.907	13.678	-35.342	4.984	0.846	0.10505
52	2.53	23.26	39.875	-10.832	29.043	50.707	12.428	-34.092	4.82	0.493	0.087143

53	2.356	25.11	35.675	-12.232	23.443	47.907	12.878	-37.342	5.52	0.972	0.11428
54	2.472	23.86	38.475	-12.232	26.243	50.707	11.628	-36.092	5.33	0.6	0.095373
55	2.594	22.67	41.275	-12.232	29.043	53.507	10.44	-34.9	5.367	0.117	0.07891
56	2.53	23.26	39.875	-13.632	26.243	53.507	9.628	-36.9	5.864	0.205	0.087143
57	2.097	28.47	29.043	0	29.043	29.043	28.47	-28.47	5.556	0	0.171382
58	2.046	29.25	27.643	-1.4	26.243	29.043	27.85	-30.65	5.9	0.184	0.185593
59	1.995	30	26.243	0	26.243	26.243	30	-30.00	6.21	0	0.20094
60	2.3	25.77	34.275	-13.63	20.643	47.907	12.14	-39.4	6.24	1.132	0.125
61	2.41	24.51	37.075	-13.63	23.443	50.707	10.878	-38.14	5.86	0.706	0.10505
62	2.472	23.86	38.475	-15.032	23.443	53.507	8.828	-38.89	6.38	0.29	0.095373
63	2.356	25.11	35.675	-15.032	20.643	50.707	10.078	-40.142	6.59	0.841	0.11428
64	2.41	24.51	37.075	-16.43	20.643	53.507	8.078	-40.94	7.1	0.398	0.10505
65	2.3	25.77	34.275	-16.432	17.843	50.707	9.338	-42.202	7.04	0.92	0.125
66	1.944	30.95	24.843	-1.4	23.443	26.243	29.55	-32.35	6.53	0.183	0.2175
67	1.895	31.85	23.443	0	23.433	23.443	31.85	31.85	6.822	0	0.235
68	2.3	25.77	34.275	-19.232	15.043	53.507	6.538	-45.00	8.22	0.541	0.125
69	1.846	32.81	22.043	-1.4	20.643	23.443	31.41	-34.2	7.263	0.272	0.253
70	1.8	33.81	20.643	0	20.643	20.643	33.81	-33.81	7.67	0	0.2715

Table (2) Characteristics Calculations for ($P_{amb.}$=1.52 bar)

Point No.	M	μ	ν	θ	C_I	C_{II}	$\theta+\mu$	$\theta-\mu$	X(mm)	Y(mm)	P(Mpa)
1	2.64	22.26	42.307	14	56.307	28.307	36.26	-8.26	0	1.65	0.0735
2	2.64	22.26	42.307	11.2	53.507	31.107	33.46	-11.06	0	1.32	0.0735
3	2.64	22.26	42.307	8.4	50.707	33.907	31.2	-13.86	0	0.99	0.0735
4	2.64	22.26	42.307	5.6	47.907	36.707	27.86	-16.66	0	0.66	0.0735
5	2.64	22.26	42.307	2.8	45.107	39.507	25.06	-19.46	0	0.33	0.0735
6	2.64	22.26	42.307	0	42.107	42.307	22.26	-22.26	0	0	0.0735
7	2.7	21.74	43.707	12.6	56.307	31.107	34.34	-9.14	0.4	1.5888	0.067
8	2.7	21.74	43.707	9.8	53.507	33.907	31.54	-11.94	0.406	1.237	0.067
9	2.7	21.74	43.707	7	50.707	36.707	28.74	-14.74	0.416	0.884	0.067
10	2.7	21.74	43.707	4.2	47.907	39.507	29.94	-17.54	0.3985	0.53743	0.067
11	2.7	21.74	43.707	1.4	45.107	42.307	23.14	-20.34	0.423	0.177	0.067
12	2.176	27.36	31.105	0	31.105	31.107	27.36	-27.36	0.711	1.74	0.152
13	2.769	21.17	45.107	11.2	56.307	33.907	32.37	-9.97	0.848	1.5126	0.06018
14	2.769	21.17	45.107	8.4	53.507	36.707	29.57	-12.77	0.8675	1.136	0.06018
15	2.769	21.17	45.107	5.6	50.707	39.507	26.77	-15.57	0.832	0.77135	0.06018
16	2.769	21.17	45.107	2.8	47.907	42.307	23.97	-18.37	0.8868	0.3855	0.06018
17	2.769	21.17	45.107	0	45.107	45.107	21.17	-21.17	0.89	0	0.06018
18	2.23	26.64	32.506	-1.4	31.105	33.907	25.24	-28.04	0.99	1.59	0.1392
19	2.836	25.95	33.906	-2.8	31.105	36.707	23.15	-28.75	1.37	1.384	0.12764
20	2.836	20.64	46.507	7	53.507	39.507	27.64	-13.64	1.33	1.03	0.054084
21	2.836	20.64	46.507	4.2	50.707	42.307	24.84	-16.44	1.3866	0.6123	0.054084
22	2.836	20.64	46.507	1.4	47.907	45.107	22.04	-9.62	1.486	0.236	0.054084
23	2.176	27.36	31.105	-2.8	28.303	33.907	24.56	-30.16	1.297	1.726	0.152
24	2.23	26.64	32.506	-1.4	31.105	33.907	25.24	-28.04	0.989	1.59	0.1392
25	2.285	25.95	33.906	-2.8	31.105	36.707	23.15	-28.75	1.37	1.384	0.12764
26	2.23	26.64	32.505	-5.6	28.303	36.707	21.04	-32.24	1.664	1.5	0.1392
27	2.176	27.36	31.105	-5.6	25.505	36.707	21.76	-32.96	1.952	1.67	0.152
28	2.285	25.95	33.905	-5.6	28.303	39.507	20.35	-31.55	1.98	1.3	0.12764
29	2.34	25.3	35.306	-4.2	31.105	39.507	21.1	-29.125	1.7	1.198	0.11719
30	2.9	20.17	47.907	5.6	53.507	42.307	25.77	-14.57	1.947	0.875	0.04937
31	2.9	20.17	47.907	2.8	50.707	45.107	22.97	-17.37	1.967	0.436	0.04937

32	2.9	20.17	47.907	0	47.907	47.907	20.17	-20.17	2.373	0	0.04937
33	2.977	19.63	49.307	1.4	50.707	47.907	21.03	-18.23	2.8114	0.165	0.043764
34	3.05	19.14	50.707	0	50.707	50.707	19.14	-19.14	3.3	0	0.04245
35	2.4	24.62	36.707	-5.6	31.105	42.307	19	-30.2	2.133	0.9515	0.1067
36	2.977	19.63	49.307	4.2	53.507	42.307	23.83	-15.43	2.586	0.704	0.043764
37	2.34	25.3	35.305	-7	28.303	45.107	18.3	-32.3	2.4	1.04	0.11719
38	2.4	24.6	36.705	-8.4	28.303	39.507	16.22	-33.02	2.8	0.783	0.1067
39	2.4	24.62	36.475	-8.4	28.303	45.107	16.22	-33.02	2.8	0.781	0.1067
40	3.05	19.14	50.707	2.8	53.507	47.907	21.94	-16.34	3.51	0.44	0.04245
41	2.176	27.36	31.105	-8.4	22.703	39.507	18.96	-35.76	2.74	1.57	0.152
42	2.23	26.64	32.505	-9.8	22.703	42.307	16.838	-36.44	3.146	1.276	0.1392
43	2.285	25.95	33.905	-11.2	22.703	45.107	14.75	-37.15	3.53	0.986	0.12764
44	2.34	25.3	35.305	-12.6	22.703	47.907	12.698	-37.9	4.03	0.6	0.11719
45	3.125	18.66	52.107	1.4	53.507	50.707	20.06	-17.26	4.06	0.272	0.03658
46	3.202	18.21	53.507	0	53.507	53.507	18.21	-18.21	4.91	0	0.03155
47	2.176	27.36	31.105	-11.2	19.903	42.307	16.16	-38.56	3.63	1.42	0.152
48	2.23	26.64	32.505	-12.6	19.903	45.107	14.04	-39.24	4.015	1.11	0.1392
49	2.285	25.95	33.905	-14	19.903	47.907	11.95	-39.95	4.515	0.706	0.12764
50	2.4	24.62	36.705	-14	22.703	50.707	10.62	-38.62	4.346	0.35	0.1067
51	2.34	25.3	37.075	-15.4	19.903	50.707	9.899	-40.7	4.83	0.4378	0.11719
52	2.176	27.36	39.875	-14	17.103	45.107	13.36	-41.36	4.5	1.227	0.152
53	2.23	26.64	35.675	-15.4	17.103	47.907	11.238	-42.04	4.98	0.8	0.1392
54	2.176	27.36	31.105	-16.8	14.3	47.907	10.56	-44.16	5.61	0.92	0.152
55	2.23	26.64	32.505	-18.2	14.303	50.707	8.44	-44.84	5.29	0.51	0.13724
56	2.176	27.36	31.105	-19.6	11.505	50.707	7.758	-46.96	6.38	0.66	0.152
57	2.456	24	38.105	-15.4	22.703	53.507	8.6	-39.4	4.8	0.024	0.09717
58	2.4	24.62	36.705	-16.8	19.903	53.507	7.82	-41.42	5.244	0.087	0.1067
59	1.77	34.36	19.903	0	19.903	19.903	34.36	-34.36	5.343	0	0.2842
60	2.285	25.95	33.905	-19.6	14.505	53.507	6.35	-45.55	5.67	0.59	0.12764
61	1.676	36.64	17.103	-2.8	14.505	19.903	33.84	-39.44	5.9	0.378	0.3257124
62	2.23	26.64	32.506	-21	11.505	53.507	5.64	-47.64	6.38	0.664	0.1392
63	1.58	39.22	14.303	0	14.303	14.303	39.22	-39.22	6.32	0	0.378
64	1.486	42.3	11.505	0	11.505	11.505	42.3	-42.3	7.04	0	0.433645
65	2.176	25.36	31.105	-22.4	8.703	53.507	4.96	-49.76	6.37	0.663	0.152

Table (3) Characteristics Calculations for ($P_{amb.}$=1.75 bar)

Point No.	M	μ	ν	θ	C_I	C_{II}	$\theta+\mu$	$\theta-\mu$	X(mm)	Y(mm)	P(Mpa)
1	2.64	22.26	42.307	14	56.307	28.307	36.26	-8.26	0	1.65	0.0735
2	2.64	22.26	42.307	11.2	53.507	31.107	33.46	-11.06	0	1.32	0.0735
3	2.64	22.26	42.307	8.4	50.707	33.907	31.2	-13.86	0	0.99	0.0735
4	2.64	22.26	42.307	5.6	47.907	36.707	27.86	-16.66	0	0.66	0.0735
5	2.64	22.26	42.307	2.8	45.107	39.507	25.06	-19.46	0	0.33	0.0735
6	2.64	22.26	42.307	0	42.107	42.307	22.26	-22.26	0	0	0.0735
7	2.7	21.74	43.707	12.6	56.307	31.107	34.34	-9.14	0.4	1.5888	0.067
8	2.7	21.74	43.707	9.8	53.507	33.907	31.54	-11.94	0.406	1.237	0.067
9	2.7	21.74	43.707	7	50.707	36.707	28.74	-14.74	0.416	0.884	0.067
10	2.7	21.74	43.707	4.2	47.907	39.507	29.94	-17.54	0.3985	0.53743	0.067
11	2.7	21.74	43.707	1.4	45.107	42.307	23.14	-20.34	0.423	0.177	0.067
12	2.084	28.67	28.66	-2.65	26.01	31.107	26	-31.32	0.611	1.8113	0.175
13	2.769	21.17	45.107	11.2	56.307	33.907	32.37	-9.97	0.848	1.5126	0.06018
14	2.769	21.17	45.107	8.4	53.507	36.707	29.57	-12.77	0.8675	1.136	0.06018
15	2.769	21.17	45.107	5.6	50.707	39.507	26.77	-15.57	0.832	0.77135	0.06018
16	2.769	21.17	45.107	2.8	47.907	42.307	23.97	-18.37	0.8868	0.3855	0.06018

17	2.769	21.17	45.107	0	45.107	45.107	21.17	-21.17	0.89	0	0.06018
18	2.132	27.97	29.96	-3.95	26.01	33.907	24	-31.92	0.98	1.584	0.16227
19	2.836	20.64	46.507	9.8	56.307	36.707	30.45	-10.84	1.3575	1.42	0.054084
20	2.186	27.23	31.36	-5.35	26.01	36.707	21.88	-32.6	1.29	1.387	0.14913
21	2.836	20.64	46.507	7	53.507	39.507	27.64	-13.64	1.33	1.03	0.054084
22	2.836	20.64	46.507	4.2	50.707	42.307	24.84	-16.44	1.3866	0.6123	0.054084
23	2.176	20.64	31.105	1.4	47.907	45.107	22.04	-9.62	1.486	0.236	0.054084
24	2.084	28.67	28.66	-5.25	23.41	33.907	23.423	-33.92	1.38	1.76	0.175
25	2.136	27.91	30.05	-6.65	23.41	36.707	21.26	-34.56	1.66	1.567	0.1613
26	2.24	26.52	32.76	-6.75	26.01	39.507	19.77	-33.26	1.635	1.164	0.13704
27	2.9	20.17	47.907	5.6	53.507	42.307	25.77	-14.57	1.947	0.875	0.04937
28	2.9	20.17	47.907	2.8	50.707	45.107	22.97	-17.37	1.967	0.436	0.04937
29	2.9	20.17	47.907	0	47.907	47.907	20.17	-20.17	2.373	0	0.04937
30	2.9	28.67	28.66	-8.05	20.61	36.707	20.623	-36.72	1.98	1.69	0.175
31	2.084	27.18	31.46	-8.05	23.41	39.507	19.13	-35.23	2.035	1.3	0.1482
32	2.19	28.67	28.66	-10.85	17.81	39.507	17.823	-39.52	2.8	1.55	0.175
33	2.084	25.83	34.16	-8.15	26.01	42.307	17.68	-33.98	2.024	0.906	0.12574
34	2.295	19.63	49.307	4.2	53.507	45.107	23.83	-15.43	2.586	0.704	0.043764
35	2.295	25.83	34.16	-8.15	26.01	42.307	17.68	-33.98	2.075	0.926	0.12574
36	2.977	19.63	49.307	1.4	50.707	47.907	21.03	-18.23	2.8114	0.165	0.04245
37	2.244	26.47	32.86	-9.45	23.41	42.307	17.02	-35.92	2.415	1.03	0.13619
38	2.084	28.67	28.66	-13.647	15.013	42.307	15.023	-42.32	2.612	1.374	0.175
39	2.3	25.78	34.26	-10.85	23.41	45.107	14.93	-36.63	2.77	0.769	0.12476
40	3.05	19.14	50.707	2.8	53.507	47.907	21.94	-16.34	3.51	0.44	0.04245
41	3.05	19.14	50.707	0	50.707	50.707	19.14	-19.14	3.3	0	0.04245
42	2.136	27.91	30.06	-15.05	15.013	45.107	12.863	-42.96	3.95	1.06	0.16126
43	2.084	28.67	28.66	-16.45	12.21	45.107	12.223	-45.12	4.4	1.161	0.175
44	2.19	27.18	31.46	-16.45	15.013	47.907	10.733	-43.63	4.35	0.685	0.1482
45	3.125	18.66	52.107	1.4	53.507	50.707	20.06	-17.26	4.065	0.272	0.03658
46	3.202	18.21	53.507	0	53.507	53.507	18.21	-18.21	4.915	0	0.03155
47	2.283	25.93	32.86	-17.85	15.013	50.707	8.083	-43.78	4.633	0.415	0.128124
48	2.136	27.91	30.06	-17.85	12.21	47.907	10.06	-45.76	4.79	0.766	0.16126
49	2.084	28.67	28.66	-19.25	9.41	47.907	9.423	-47.92	5.34	0.86	0.175
50	2.19	27.18	31.46	-19.25	12.21	50.707	7.93	-46.43	5.07	0.476	0.1482
51	2.283	25.93	32.86	-20.65	12.21	53.507	5.2815	-46.58	5.42	0.105	0.128124
52	1.51	41.47	12.21	0	12.21	12.21	41.47	-41.47	5.53	0	0.41883
53	2.136	27.91	30.06	-20.65	9.41	50.707	7.2615	-48.56	5.62	0.55	0.16126
54	2.084	28.67	28.66	-22.05	6.61	50.707	6.623	-50.72	6.03	0.6	0.175
55	2.19	27.18	31.46	-22.05	9.41	53.507	5.1315	-49.23	5.965	0.155	0.1482
56	1.415	44.97	9.41	0	9.41	9.41	44.97	-44.97	6.11	0	0.4799
57	2.136	27.91	30.06	-23.45	6.61	53.507	4.46	-51.36	6.34	0.188	0.16126
58	1.316	49.45	6.61	0	6.61	6.61	49.455	-49.455	6.5	0	0.55087
59	2.084	28.67	28.66	-24.85	3.81	53.507	3.823	-53.52	6.89	0.228	0.175